Quark Degeneracy and the Lower Mass Gap

Gregory L. Frazier

Abstract

The observed deficit of compact objects between $\sim$2.5 and $\sim$5 $M_\odot$—the lower mass gap—has no widely accepted physical explanation. We propose that the gap is the signature of the phase transition from neutron-degenerate to quark-degenerate matter, and present four lines of evidence: (1) the TOV equations predict the step-function jump in gravitational mass at the neutron$\rightarrow$quark transition; (2) pulsars above the 2 $M_\odot$ stability limit are observed only at fast spin rates, consistent with centrifugal support delaying collapse to black hole; (3) failed supernovae confirm that cores well below 5 $M_\odot$ collapse; and (4) analysis of LIGO black hole merger data reveals spin-dependent mass deficits consistent with black holes being structured matter (versus being singularities). Stellar objects (neutron stars, red supergiant cores) of $\sim$2 $M_\odot$ in size collapse to form black holes, and the smallest observed black hole is over 5 $M_\odot$. There is no baryonic mass gap—the gap is in the observed, gravitational mass and is an inevitable result of the increased pressure that results from the collapse. And the existence of pressure means that black holes cannot be singularities.

Independent researcher. The author thanks Claude (Anthropic) for assistance with analysis and manuscript preparation.

1. Introduction

Gravitational-wave and X-ray observations reveal a gap in the mass spectrum of compact objects. Neutron stars with dynamically measured masses cluster below $\sim$2.5 $M_\odot$ (Lattimer 2026), while black holes in X-ray binaries begin near $\sim$5 $M_\odot$ (Bailyn et al. 1998). The deficit of objects between these limits is the *lower mass gap*.

The reality and origin of the gap have been debated for two decades. Bailyn et al. (1998) first identified the clustering of X-ray binary black holes above $\sim$5 $M_\odot$; Özel et al. (2010) argued on statistical grounds that the gap is real and not a selection effect, and Farr et al. (2011) reached the same conclusion with a Bayesian analysis. Kreidberg et al. (2012) countered that systematic errors in X-ray binary mass measurements could partially fill the gap. On the theoretical side, Fryer et al. (2012) showed that rapid supernova explosion mechanisms can produce a gap by ejecting the envelope before significant fallback, while delayed mechanisms fill it in. More recently, the LIGO–Virgo detection of GW190814—a merger whose 2.6 $M_\odot$ secondary sits squarely in the gap (Abbott et al. 2020)—and population synthesis studies (Zevin et al. 2020) have renewed the question of whether the gap is truly empty or merely underpopulated. No consensus has emerged on the physical origin of the deficit.

We propose that the lower mass gap is the signature of a phase transition. When a neutron star exceeds the Tolman-Oppenheimer-Volkoff (TOV) stability limit, its matter collapses from neutron degeneracy to quark degeneracy, producing a step-function increase in compactness, pressure, and thus gravitational mass. But the TOV equations not only predict the increase in gravitational mass—they also predict that, at the point where a neutron star collapses, the result is a black hole. The pressure contribution to gravitational mass cannot operate if the mass exists as a dimensionless point. As such, this explanation requires that black holes are not singularities but structured bodies—objects with a real equation of state, finite volume, and internal pressure inside the event horizon. This is a testable requirement; if black holes have internal structure, their mergers should exhibit signatures inconsistent with point-mass predictions. Thus we present four lines of evidence: TOV equations predict the gap (§2); massive pulsars (§3.1) and the pulsar population (§3.2) show the expected spin-dependent disappearance; failed supernovae independently confirm sub-5 $M_\odot$ collapse of objects to black holes (§3.3); and LIGO merger remnants carry spin signatures consistent with structured matter, in contrast to point singularities (§4).

2. TOV Equation Analysis

The Tolman–Oppenheimer–Volkoff equations (Tolman 1939; Oppenheimer and Volkoff 1939) govern the hydrostatic structure of a self-gravitating, spherically symmetric body in general relativity. In particular, the pressure gradient equation,

$$\frac{dP}{dr} = -\frac{\left(\rho + P/c^2\right)\left(m + 4\pi r^3 P/c^2\right) G}{r\left(r - 2Gm/c^2\right)}, \tag{1}$$

contains terms in which the pressure P itself contributes to the source of gravity. As a consequence, the gravitational mass of a compact star—the mass that determines its orbit and gravitational field—exceeds its baryonic (rest) mass: $M_{\rm g} > M_{\rm b}$. We define $M_{\rm g}$ as the total gravitational mass enclosed at the stellar surface. The baryonic mass $M_{\rm b}$ is defined so as to isolate the ground-state structural energy of each matter type, excluding the internal kinetic energy that generates pressure. For neutron-star matter, $M_{\rm b}$ is the integral of the baryon rest-mass density ρ_0 over coordinate volume—the mass the baryons would have if dispersed to infinity with zero internal energy. For quark-star matter, $M_{\rm b}$ is the integral of the bag vacuum energy density $4B/c^2$ over coordinate volume—the QCD vacuum cost of creating the quark-matter volume, with no quark kinetic contribution. Both definitions strip the internal energy that generates pressure and keep only the structural ground state. The difference $M_{\rm g} - M_{\rm b}$ then measures pressure's contribution to the gravitating mass for both matter types, and grows with compactness.

The relationship between pressure, density, and composition is encoded in the equation of state (EOS). For neutron-star matter, we adopt six finite-temperature nuclear EOS tables from the `stellarcollapse.org` repository (O'Connor and Ott 2010), evaluated on the cold, beta-equilibrated slice: LS180, LS220, and LS375 (Lattimer and Swesty 1991), SFHo (Steiner, Fischer, and Hempel 2013), DD2 (Typel et al. 2010), and HShen (Shen et al. 1998). These span the range from soft (LS180, $K = 180$ MeV) to stiff (LS375, $K = 375$ MeV) nuclear incompressibilities, producing maximum neutron-star masses of roughly 2.0–3.0 $\mathrm{M}_\odot$. For quark-star matter we use the MIT bag model (Chodos et al. 1974) with three representative bag constants, $B = 60$, 100, and 160 $\mathrm{MeV/fm^3}$, spanning the range from soft to stiff quark matter. These produce maximum gravitational masses of roughly 2.0, 1.6, and 1.2 $\mathrm{M}_\odot$, respectively. While pure quark stars remain theoretical, recent Bayesian analyses of neutron-star observations find strong evidence for quark-matter cores above $\sim$2 $\mathrm{M}_\odot$ (Annala et al. 2020).

Figure 1A shows the standard mass–radius diagram obtained by integrating Eq. (1) across a range of central pressures for each EOS. The neutron-star branches span radii of $\sim$11–15 km, while the quark-star branches are more compact, reaching $\sim$7–11 km at maximum mass depending on B. Both families terminate at a maximum gravitational mass beyond which no stable equilibrium exists.

The key result is shown in Figure 1B, which plots $M_{\rm g}$ against $M_{\rm b}$. Every TOV solution sits above the $M_{\rm g} = M_{\rm b}$ line; the departure grows with compactness. The neutron-star curves (solid) hug the diagonal, with the pressure contribution amounting to $\sim$10–15% of $M_{\rm g}$ at maximum mass. The quark-star curves (dashed) depart dramatically: because the baryonic mass counts only the bag vacuum energy ($4B/c^2$), the entire ultrarelativistic quark kinetic energy ($3P/c^2$) appears as excess gravitational mass. At the quark-star maximum, $M_{\rm g}/M_{\rm b} \sim 1.5$–2, meaning that pressure-generated energy accounts for roughly half the gravitating mass.

The implications for the mass gap are direct. When a neutron star exceeds its TOV limit, it collapses from neutron-degenerate to quark-degenerate matter. The baryonic mass is conserved,

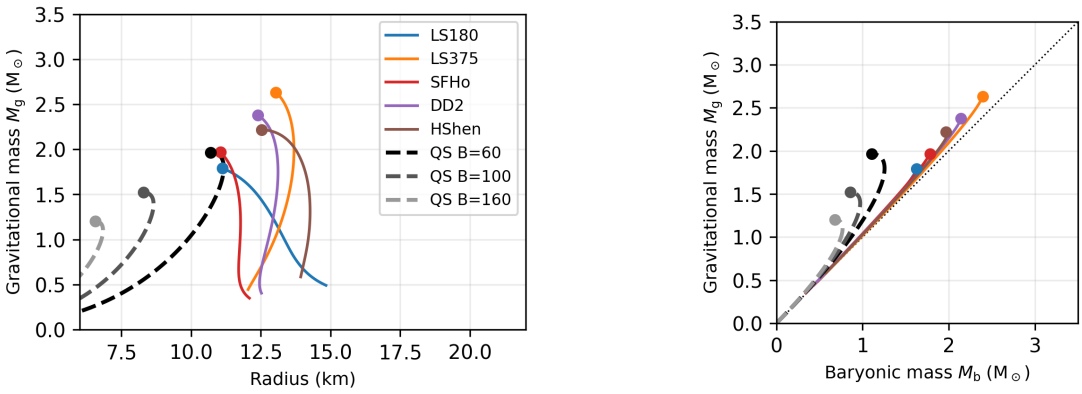

A. Gravitational Mass vs. Radius

B. Gravitational Mass vs. Baryonic Mass

FIGURE 1. Neutron and Quark Star Stable Configurations

Solid curves are the six nuclear EOS; the dashed curves are MIT bag model quark stars with $B = 60$, 100, and 160 MeV/fm^3. For a given baryonic mass M_b, quark stars have greater gravitational mass M_g than do neutron stars.

but because the resulting quark star is more compact, its pressure contribution to M_g is larger: the gravitational mass jumps upward. The lower mass gap—the observed deficit of compact objects between $\sim$2.5 and $\sim$5 $M_\odot$ (Özel et al. 2010; Farr et al. 2011)—is the signature of this transition, spanning from the pre-collapse neutron-star M_g to the post-collapse quark-star M_g. Crucially, the post-collapse gravitational mass exceeds the maximum stable quark-star solution: the object is not a quark star but a black hole. Yet, the smallest observed black holes are over 5 $M_\odot$, suggesting that black holes have a pressure component to their M_g, which in turn implies that they are coherent stellar objects—they are quark stars.

The spread of EOS and bag constants in Fig. 1 reflects current uncertainty in dense-matter physics; the precise behavior of matter at these densities is not yet known. Nonetheless, the qualitative picture is robust. Both families show a steepening M_g–M_b relationship with increasing baryonic mass, and quark stars consistently exhibit a far larger pressure contribution to M_g than neutron stars at comparable M_b.

This pressure contribution to M_g is not merely a theoretical refinement; it is an observable that distinguishes structured objects from singularities. A point singularity has zero volume, no equation of state, and no internal pressure—the TOV mechanism cannot operate. If black holes are singularities, their gravitational mass equals their baryonic mass by construction. The fact that the smallest observed black holes sit well above the neutron star maximum implies a pressure contribution, and therefore internal structure.

That said, the TOV analysis demonstrates only that a phase transition *would* produce a mass gap whose endpoint is a black hole; it does not, by itself, show that neutron stars *do* collapse. Indeed, the absence of a stable post-collapse solution might be read as evidence against collapse. Observational evidence that collapse is occurring is presented in the following section.

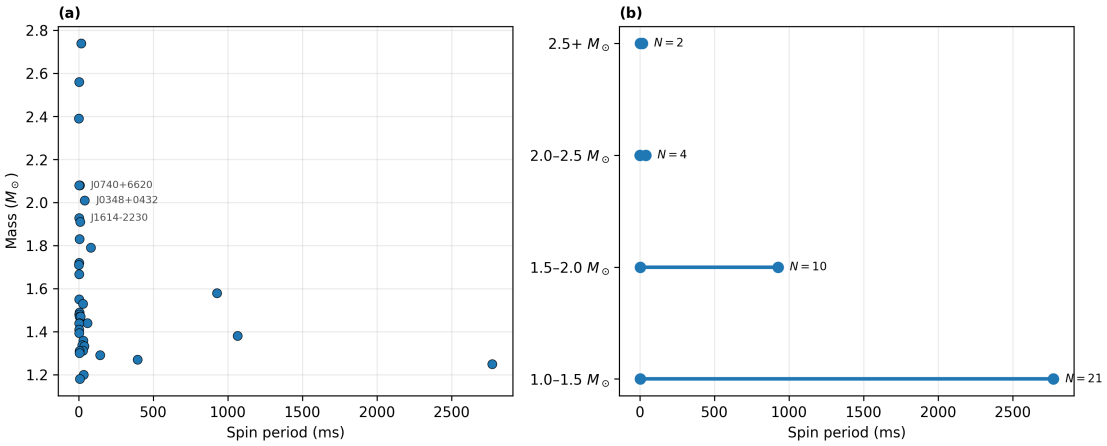

FIGURE 2. Mass vs. Spin Period, Pulsars with Known Mass

Examined 37 pulsars with dynamical mass measurements. (a) Scatter plot of 37 pulsars with known mass. No pulsar above 1.6 $M_\odot$ has a slower period than 80 ms. (b) Period range per mass-bin: horizontal segments span from the fastest to the slowest period in each bin, with sample size annotated. The fastest periods are comparable across all bins (1.61–2.56 ms), but the slowest period drops from 2773 ms to 16.8 ms as mass increases. Note also that the number of pulsars in each bin decreases as the masses increase.

3. Observational Evidence for Collapse

The TOV analysis predicts that neutron stars exceeding the stability limit collapse through the mass gap into quark-degenerate configurations. This section presents three independent lines of evidence that such collapses are occurring: the spin-dependent disappearance of massive pulsars, the thinning of the pulsar population at long spin periods, and the failed-supernova phenomenon in red supergiants.

3.1. Pulsars with Known Mass

We assemble a sample of 37 pulsars with dynamically measured masses from the `stellarcollapse.org` compilation (O'Connor and Ott 2010), cross-matched with spin periods from the ATNF Pulsar Catalogue (Manchester et al. 2005). The sample spans 1.18–2.74 $M_\odot$ and includes four binary categories: NS–WD (21 systems), NS–NS (7), X-Ray/Optical (2), and NS–MS (3). Three of the most precisely measured high-mass pulsars—J0740+6620 (2.08 ± 0.07 $M_\odot$; Cromartie et al. 2020), J0348+0432 (2.01 ± 0.04 $M_\odot$), and J1614−2230 (1.928 ± 0.017 $M_\odot$)—anchor the high end of the distribution.

Figure 2 reveals the key pattern. When the sample is binned by mass, the fastest spin period in each bin is comparable (1.61–2.56 ms), showing that millisecond pulsars exist at all masses. But the slowest period shrinks dramatically: from 2773.5 ms in the 1.0–1.5 $M_\odot$ bin down to 16.8 ms above 2.5 $M_\odot$. Massive pulsars are found exclusively at fast spin rates; no slowly rotating high-mass neutron star has been observed.

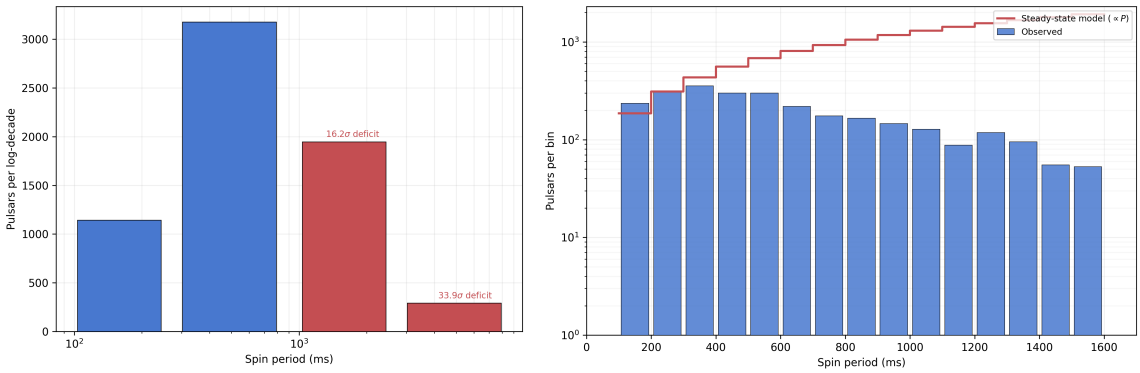

A. Density per log-decade

B. Fixed-width bins vs. model

FIGURE 3. Period Distribution of Normal Pulsars ($P \geq 100$ ms)

(a) Pulsars per log-decade in four logarithmically spaced bins. Blue bars are consistent with a non-decreasing density; red bars fall below the peak, with Poisson significance annotated. (b) Observed counts in 100 ms bins (blue) compared with the steady-state dipole spin-down prediction (count $\propto P$, red step line, normalised at 200–300 ms). Note the logarithmic vertical axis for (b).

This pattern is consistent with spin providing centrifugal support that delays collapse past the TOV stability limit. As pulsars spin down, those with the highest baryonic mass cross the stability boundary first, disappearing from the observable population. Only those massive pulsars that still retain fast spin remain visible. A Spearman rank correlation confirms the trend: $\rho = -0.41$ ($p = 1.1 \times 10^{-2}$), indicating a statistically significant negative association between mass and spin period.

That said, these 37 pulsars are the subset with dynamically measured masses—a small, heterogeneous sample. The next subsection uses the full ATNF pulsar catalogue to test this interpretation with stronger statistics.

3.2. Pulsar Population Analysis

The preceding analysis showed that among pulsars with measured masses, the most massive are found exclusively at fast spin rates. If larger pulsars collapse as they spin down, the effect should leave a clear imprint on the period distribution of the full pulsar population.

We draw 4286 pulsars from the ATNF Pulsar Catalogue (Manchester et al. 2005) and restrict the sample to the 3305 normal (non-recycled) pulsars with $P \geq 100$ ms. Under magnetic dipole braking ($P\dot{P} \approx$ const), the period derivative $\dot{P} \propto 1/P$, so pulsars traverse a given period interval more slowly at long periods. The dwell time in an interval dP scales as $P\,dP$, and in a steady-state population with constant birth rate the number density per log-decade of period should be non-decreasing.

Figure 3A tests this prediction. The density rises from 1142 pulsars per decade in the 100–300 ms bin to a peak of 3175 in the 300–1000 ms bin, then drops precipitously: 1947 in the 1000–3000 ms bin (a 16.2σ deficit relative to the non-decreasing null) and just 293 in the 3000–

10000 ms bin (33.9σ). Figure 3B shows the same data in fixed-width bins alongside the steady-state prediction. The observed counts fall exponentially while the model rises linearly; by 3 s the gap exceeds an order of magnitude.

The conventional explanation for the missing long-period pulsars is luminosity death: the cessation of coherent radio emission below a critical spin-down power (Faucher-Giguère and Kaspi 2006). However, the death line operates at $P \gtrsim 5$ s for typical magnetic fields and so does not account for a population decline that is already observable at 0.1 s and is distributed across the entire range of pulsar spin periods. Population synthesis studies have invoked magnetic field decay to fill the gap, but the required timescales are uncertain and Faucher-Giguère and Kaspi (2006) found no evidence for significant field decay over pulsar lifetimes. Most recently, Sautron et al. (2024) showed that a death line is not necessary to reproduce the observed P–$\dot{P}$ diagram: their simulations with and without a death line are statistically indistinguishable once the maximum pulsar age is capped at $\sim 4 \times 10^7$ yr. What is required is simply that old pulsars are absent—but the physical reason for their absence remains unexplained in that framework.

The collapse hypothesis of §3.1 offers a natural explanation for observed population dynamics. As pulsars spin down, those with baryonic masses near the TOV limit lose centrifugal support and collapse to quark stars (black holes), physically removing them from the observable population. This predicts a gradual thinning of the population that begins well before the nominal death line—precisely the pattern seen in Figures 3A and 3B. It further predicts that the deficit should be strongest among the most massive pulsars, a test that targeted mass measurements at long periods could address.

3.3. The Red Supergiant Problem

The preceding subsections established that pulsars are disappearing from the observable population as they spin down—evidence that compact objects with baryonic mass well below 5 $M_\odot$ are collapsing to form black holes. Here we examine a completely independent line of evidence that points to the same conclusion.

Red supergiants (RSGs) are massive evolved stars in the final stages of nuclear burning, with initial (zero-age main-sequence) masses of roughly 8–25 $M_\odot$. Stars in this range are expected to end their lives as core-collapse supernovae. However, Smartt et al. (2009) analysed pre-explosion images of a volume-limited sample of Type II-P supernovae and found that no progenitor more massive than 16.5 ± 1.5 $M_\odot$ had been identified—despite RSGs with masses up to $\sim$25 $M_\odot$ being well documented in the Local Group. An expanded sample of 45 progenitors confirmed the deficit: 13 high-luminosity progenitors were expected under a Salpeter initial mass function, but only one was found (Smartt 2015). This discrepancy—the absence of supernova progenitors in the $\sim$17–25 $M_\odot$ range—is known as the *red supergiant problem*.

The natural explanation is that the most massive RSGs do not produce visible supernovae: their cores collapse directly to black holes, with the stellar envelope falling back rather than being ejected.

Kochanek (2020) showed that this "failed supernova" hypothesis provides a consistent explanation for both the missing progenitors and the observed black hole mass function. A systematic search by the Large Binocular Telescope survey, monitoring luminous stars in 27 nearby galaxies over 11 years, estimates that $16^{+23}_{-12}\%$ of core-collapse events produce failed supernovae (Neustadt and Kochanek 2021).

Two candidate failed supernovae have now been identified observationally. NGC 6946-BH1, a $\sim$25 $M_\odot$ red supergiant, underwent a brief optical outburst in 2009 and then vanished; by 2015 it was undetectable in optical light (Adams et al. 2017), though subsequent JWST imaging revealed that the pre-disappearance source was a blend of at least three objects, complicating the interpretation (Beasor et al. 2024). The clearer case is M31-2014-DS1, a hydrogen-depleted supergiant in the Andromeda Galaxy (De et al. 2026). With an initial mass of $\sim$13 $M_\odot$—notably below the RSG problem threshold, extending the failed-supernova phenomenon to lower masses—and a terminal mass of $\sim$5 $M_\odot$, this star faded by a factor of $\gtrsim 10^4$ in optical light between 2017 and 2022 with no associated supernova. Modelling indicates that $\sim$98% of the stellar mass collapsed or fell back, forming a $\sim$5 $M_\odot$ black hole.

The implications for the mass gap are direct. Stellar evolution models show that the iron core mass at the point of collapse is $\sim$1.3–1.8 $M_\odot$ across the entire range from 8 to 25 $M_\odot$ (Woosley, Heger, and Weaver 2002; Sukhbold et al. 2016). This is the mass that actually undergoes gravitational collapse; subsequent accretion of envelope material occurs only after the compact remnant has formed. Even the helium core—an upper bound on the material that can plausibly fall back—is only $\sim$4–9 $M_\odot$ for stars of 15–25 $M_\odot$. In every case, the baryonic mass of the collapsing core is certainly less than 5 $M_\odot$ and most likely less than 2 $M_\odot$.

The failed-supernova evidence therefore establishes, independently of the pulsar analysis, that cores with baryonic mass well below 5 $M_\odot$—most likely $\sim$1.5 $M_\odot$—can and do collapse to form black holes. This is precisely the process proposed in §3.1 and §3.2 for pulsars that lose centrifugal support as they spin down. That the same phenomenon—black hole formation from a $\sim$2 $M_\odot$ compact core—appears in two completely unrelated astrophysical settings strengthens the case that the lower mass gap is the signature of this collapse, as predicted by the TOV analysis of §2.

4. Black Hole Merger Spin Analysis

The preceding sections established that compact objects with baryonic mass well below 5 $M_\odot$ collapse to form black holes, and that the TOV equations predict a mass gap at the neutron–quark transition. But those arguments do not, by themselves, demonstrate that black holes contain structured matter. If black holes are quark stars—compact objects with a real equation of state, finite radius, and internal pressure—then their mergers should leave observable signatures in the gravitational-wave record that differ from the predictions of the point-singularity model. The GWTC catalog (The LIGO Scientific Collaboration, The Virgo Collaboration, and The KAGRA Collaboration 2023; Abbott et al. 2023) provides exactly the data needed to test this.

Consider two models of what happens when two black holes merge. In the singularity model, each black hole is a point mass enclosed by an event horizon; the mass deficit $m_1 + m_2 - m_{\rm final}$ is energy radiated as gravitational waves. The "spin" of a Kerr black hole is a property of the spacetime geometry: angular momentum is defined as a conserved charge at spatial infinity, and the singularity itself has no moment of inertia and no internal structure for centrifugal force to act upon. In the quark star model, two physical objects collide and merge. The remnant is a spinning body with a moment of inertia, and its spin provides centrifugal support that reduces the internal pressure and therefore reduces the gravitational mass $M_{\rm g}$ relative to the conserved baryonic mass $M_{\rm b}$. No baryonic mass is converted to energy—the gravitational-wave energy comes from the rotational kinetic energy of the inspiral—and the apparent mass deficit includes a spin-induced reduction in $M_{\rm g}$.

The two models also differ in how they account for the gravitational waves observed after the merger (the "ringdown"). In the singularity model, the inspiral GWs are driven radiation, sourced by the stress-energy of orbiting masses; but the post-merger GWs are quasi-normal modes—source-free oscillations of the Kerr geometry ringing down to equilibrium. The radiation mechanism changes at merger from matter-sourced to geometry-sourced. In the quark star model, a single mechanism operates throughout: the time-varying quadrupole moment of a physical mass distribution, first from two bodies in mutual orbit, then from a distorted remnant settling into axial symmetry. Both models predict post-merger gravitational waves—quasi-normal modes have been a prediction of the Kerr model since the 1970s—but they disagree on what is radiating.

Both models predict that the mass deficit depends on the symmetric mass ratio $\eta = m_1 m_2/(m_1 + m_2)^2$, because the orbital dynamics that govern both GW radiation and angular momentum transfer are controlled by η. We use the spinning-GR prediction as a baseline, extending Buonanno, Kidder, and Lehner (2008) by replacing the Schwarzschild ISCO binding energy with its Kerr analogue (Bardeen, Press, and Teukolsky 1972):

$$f_{\rm GR}(\eta, \chi_{\rm eff}) = e_{\rm ISCO}(\chi_{\rm eff})\,\eta + 0.498\,\eta^2, \tag{2}$$

where $e_{\rm ISCO}(\chi_{\rm eff})$ is the analytic Kerr ISCO binding energy fraction; at $\chi_{\rm eff} = 0$ it equals $1 - \sqrt{8/9} \approx 0.0572$, recovering the BKL non-spinning formula. The quark star model predicts additional deficit from spin-induced $M_{\rm g}$ reduction, proportional to the remnant spin generated.

We test this using 157 confident binary black hole events ($m_1 > 3\,{\rm M}_\odot$, $m_2 > 3\,{\rm M}_\odot$, $p_{\rm astro} > 0.5$) from the GWTC catalog, of which 154 have both a measured final mass and effective spin $\chi_{\rm eff}$. For each event we compute the remnant spin χ_f from the numerical-relativity fitting formula

$$\chi_f = L_{\rm orb}(\eta) + \frac{\chi_{\rm eff}\,(1+q^2)}{(1+q)^2}, \tag{3}$$

where $L_{\rm orb}(\eta) = 2\sqrt{3}\,\eta - 3.52\,\eta^2 + 2.58\,\eta^3$ is the orbital angular momentum contribution and the second term is the spin angular momentum contribution (assuming equal component spins

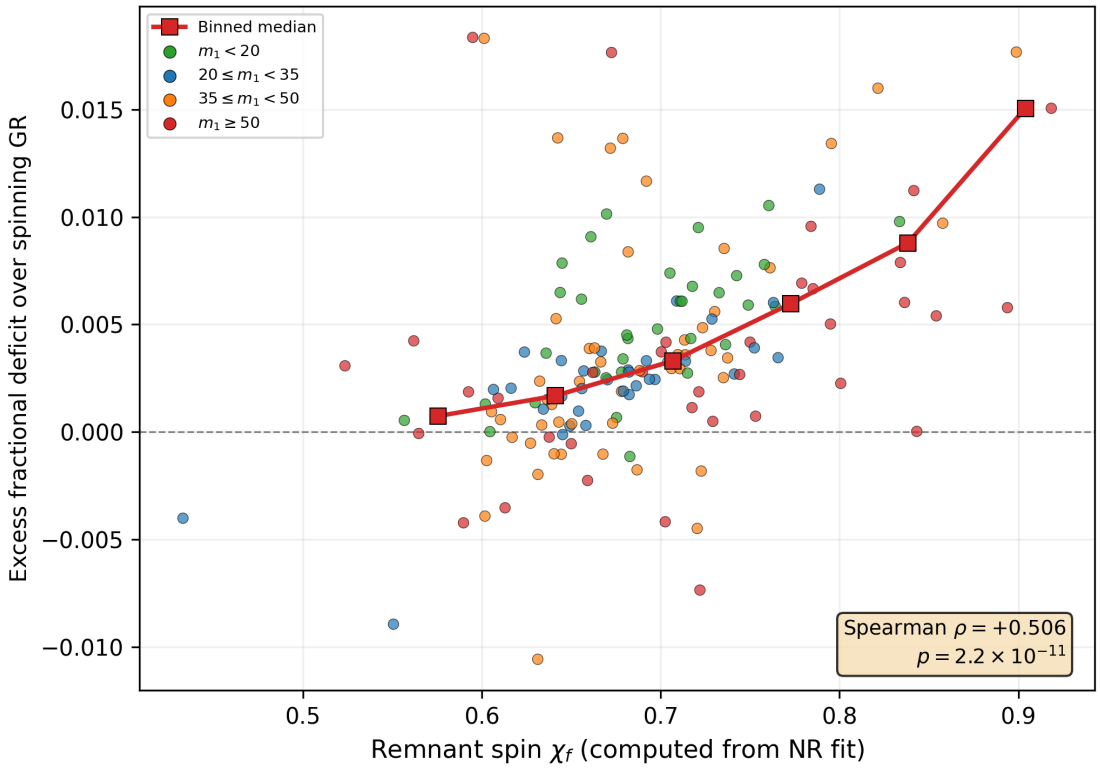

FIGURE 4. Excess Fractional Mass Deficit vs. Remnant Spin

Each point is a GWTC binary black hole merger. The excess is computed relative to the spinning GR prediction (Eq. 2). Points are coloured by primary mass m_1. Remnant spin χ_f is computed from Eq. (3). Red squares show binned medians. The Spearman correlation ($\rho = +0.506$, $p = 2.2 \times 10^{-11}$) confirms that higher remnant spin is associated with larger excess deficit.

$a_1 = a_2 = \chi_{\rm eff}$). The excess fractional deficit is then $\Delta f = f_{\rm obs} - f_{\rm GR}$, where $f_{\rm obs} = (m_1 + m_2 - m_{\rm final})/(m_1 + m_2)$.

Test 1: excess deficit vs. remnant spin. Figure 4 plots the excess fractional deficit Δf against the computed remnant spin χ_f for all 154 events. A Spearman rank correlation gives $\rho = +0.506$ ($p = 2.2 \times 10^{-11}$), a highly significant positive association. The median excess is 0.0029, and 84% of events exceed the spinning GR prediction. The binned medians trace a clear rising curve from near zero at $\chi_f \approx 0.55$ to $\sim$0.012 at $\chi_f \approx 0.85$.

The quark star model offers a direct physical mechanism for this correlation: a spinning body with internal structure experiences centrifugal support that reduces its central pressure and therefore its gravitational mass. More remnant spin means more centrifugal support and a larger apparent mass deficit. In the singularity model, the remnant's "spin" is a geometric property of the Kerr metric, with no internal structure for centrifugal force to act upon; the connection between spin and mass deficit is less direct.

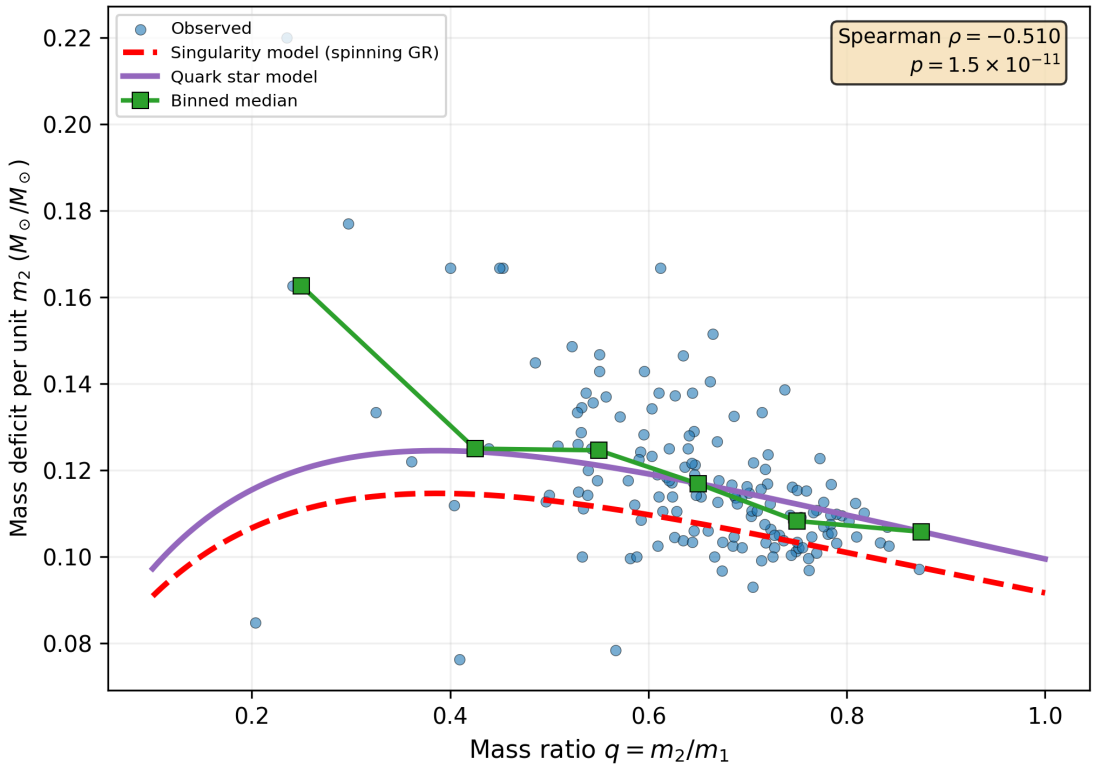

FIGURE 5. Mass Deficit per Unit m_2 vs. Mass Ratio

Blue points: observed deficit divided by m_2 for each GWTC event. Red dashed curve: singularity model (spinning GR, Eq. 2, at median $\chi_{\rm eff}$). Purple solid curve: quark star model, adding spin-induced $M_{\rm g}$ reduction with $\alpha = 0.0083$ fit from Test 1. Green squares: binned medians. The data follow the quark star prediction, not the singularity prediction ($\rho = -0.510$, $p = 1.5 \times 10^{-11}$).

A natural concern is that the Test 1 correlation might partly reflect shared η-dependence: χ_f contains $L_{\rm orb}(\eta)$ and $f_{\rm GR}$ also depends on η. In the GWTC sample, however, χ_f is dominated by the progenitor spin component $\chi_{\rm eff}(1+q^2)/(1+q)^2$ (Spearman $\rho = +0.875$ with χ_f) rather than by $L_{\rm orb}(\eta)$ ($\rho = +0.041$). More tellingly, η is *negatively* correlated with the excess ($\rho = -0.349$, $p = 9.0 \times 10^{-6}$), so the $L_{\rm orb}$ term dilutes rather than drives the Test 1 result. Using the progenitor spin component alone yields a stronger correlation ($\rho = +0.643$, $p = 2.6 \times 10^{-19}$); the partial Spearman correlation controlling for η gives $\rho = +0.556$ ($p = 7.4 \times 10^{-14}$); and the correlation is highly significant within each of three equal-sized η-tercile subsamples ($\rho \approx 0.45$–0.55 in each). There is no η-confound: the excess tracks progenitor spin, not mass-ratio geometry.

Test 2: deficit per unit m_2 vs. mass ratio. Figure 5 plots the total mass deficit per unit m_2 against the mass ratio q. The singularity model curve (red, dashed) is the spinning GR baseline (Eq. 2) evaluated at the sample median $\chi_{\rm eff} = 0.05$, normalised by m_2. The quark star model curve (purple, solid) adds the spin-induced $M_{\rm g}$ reduction, $f_{\rm QS} = f_{\rm GR} + \alpha L_{\rm orb}(\eta)^2$, using $\alpha = 0.0083$ taken directly from

the Test 1 fit—a parameter-free prediction for Test 2. Both curves share the same shape because GW radiation and spin deposition are both governed by η; the quark star curve is shifted uniformly upward because the decreasing $L_{\rm orb}^2$ at low q is offset by the increasing $1/m_2$ amplification.

The binned medians (green squares) track the quark star curve across the full range of mass ratios, sitting consistently above the singularity prediction ($\rho = -0.510$, $p = 1.5 \times 10^{-11}$). The quark star model thus accounts for both tests with one physical mechanism—centrifugal support reducing $M_{\rm g}$—and one free parameter (α) calibrated on Test 1 and applied unchanged to Test 2.

5. Conclusion

The lower mass gap between neutron stars and black holes has lacked a physical explanation. We have argued that there is no *baryonic* mass gap. The gap is in the gravitational mass (which is what is directly observable), and is the signature of the phase transition from neutron degeneracy to quark degeneracy, driven by the same pressure–gravity coupling embedded in the TOV equations. A direct implication is that black holes are not singularities but structured stellar objects with finite volume, an equation of state, and internal pressure that contributes to their gravitational mass.

Four independent lines of evidence support this picture. The TOV equations show that a neutron-to-quark transition produces a gravitational-mass jump that anticipates the observed gap (§2). Massive pulsars are found exclusively at fast spin rates, consistent with centrifugal support delaying collapse past the stability limit (§3.1). An assessment of the full observed pulsar population, for which mass information is unavailable, shows that pulsars are disappearing from the population, consistent with centrifugal support delaying collapse (§3.2). Failed supernovae confirm, independently of the pulsar evidence, that stellar cores with baryonic mass well below 5 $M_\odot$ collapse to form black holes (§3.3). Finally, LIGO merger remnants show a spin-dependent mass deficit that correlates with remnant spin and exceeds the spinning GR prediction by the amount a structured-matter model predicts—with a single free parameter calibrated on one observable and applied to a second (§4).

Several directions for future work are apparent. Targeted mass measurements of long-period pulsars could test the prediction that the spin-down disappearance is strongest among the most massive neutron stars. And the continued growth of the gravitational-wave catalog will improve the statistical power of the merger analysis presented here.

References

Abbott, R., T. D. Abbott, S. Abraham, F. Acernese, K. Ackley, C. Adams, et al. 2020. "GW190814: Gravitational Waves from the Coalescence of a 23 Solar Mass Black Hole with a 2.6 Solar Mass Compact Object." *The Astrophysical Journal Letters* 896: L44. 10.3847/2041-8213/ab960f.

Abbott, R. et al. 2023. "Open data from the third observing run of LIGO, Virgo, KAGRA, and GEO." *The Astrophysical Journal Supplement Series* 267: 29. 10.3847/1538-4365/acdc9f.

Adams, S. M., C. S. Kochanek, J. R. Gerke, K. Z. Stanek, and X. Dai. 2017. "The search for failed supernovae with the Large Binocular Telescope: confirmation of a disappearing star." *Monthly Notices of the Royal Astronomical Society* 468: 4968–4981. 10.1093/mnras/stx816.

Annala, Eemeli, Tyler Gorda, Aleksi Kurkela, Joonas Nättilä, and Aleksi Vuorinen. 2020. "Evidence for quark-matter cores in massive neutron stars." *Nature Physics* 16: 907–910. 10.1038/s41567-020-0914-9.

Bailyn, Charles D., Raj K. Jain, Paolo Coppi, and Jerome A. Orosz. 1998. "The Mass Distribution of Stellar Black Holes." *The Astrophysical Journal* 499: 367–374. 10.1086/305614.

Bardeen, James M., William H. Press, and Saul A. Teukolsky. 1972. "Rotating Black Holes: Locally Nonrotating Frames, Energy Extraction, and Scalar Synchrotron Radiation." *The Astrophysical Journal* 178: 347–370. 10.1086/151796.

Beasor, Emma R., Griffin Hosseinzadeh, Nathan Smith, et al. 2024. "JWST Reveals a Luminous Infrared Source at the Position of the Failed Supernova Candidate N6946-BH1." *The Astrophysical Journal* 964: 171. 10.3847/1538-4357/ad2df0.

Buonanno, Alessandra, Lawrence E. Kidder, and Luis Lehner. 2008. "Estimating the final spin of a binary black hole coalescence." *Physical Review D* 77: 026004. 10.1103/PhysRevD.77.026004.

Chodos, A., R. L. Jaffe, K. Johnson, Charles B. Thorn, and V. F. Weisskopf. 1974. "New extended model of hadrons." *Physical Review D* 9: 3471–3495. 10.1103/PhysRevD.9.3471.

Cromartie, H. Thankful, Emmanuel Fonseca, Scott M. Ransom, Paul B. Demorest, Zaven Arzoumanian, Harsha Blumer, Paul R. Brook, Megan E. DeCesar, Timothy Dolch, Justin A. Ellis, et al. 2020. "Relativistic Shapiro delay measurements of an extremely massive millisecond pulsar." *Nature Astronomy* 4: 72–76. 10.1038/s41550-019-0880-2.

De, Kishalay, Morgan MacLeod, Jacob E. Jencson, Elizabeth Lovegrove, et al. 2026. "Disappearance of a massive star in the Andromeda Galaxy due to formation of a black hole." *Science* 391: 689. 10.1126/science.adt4853.

Farr, Will M., Niharika Sravan, Andrew Cantrell, Laura Kreidberg, Charles D. Bailyn, Ilya Mandel, and Vicky Kalogera. 2011. "The Mass Distribution of Stellar-mass Black Holes." *The Astrophysical Journal* 741: 103. 10.1088/0004-637X/741/2/103.

Faucher-Giguère, Claude-André and Victoria M. Kaspi. 2006. "Birth and Evolution of Isolated Radio Pulsars." *The Astrophysical Journal* 643: 332–355. 10.1086/501516.

Fryer, Chris L., Krzysztof Belczynski, Grzegorz Wiktorowicz, Michal Dominik, Vicky Kalogera, and Daniel E. Holz. 2012. "Compact Remnant Mass Function: Dependence on the Explosion Mechanism and Metallicity." *The Astrophysical Journal* 749: 91. 10.1088/0004-637X/749/1/91.

Kochanek, C. S. 2020. "On the red supergiant problem." *Monthly Notices of the Royal Astronomical Society* 493: 4945–4956. 10.1093/mnras/staa605.

Kreidberg, Laura, Charles D. Bailyn, Will M. Farr, and Vicky Kalogera. 2012. "Mass Measurements of Black Holes in X-Ray Transients: Is There a Mass Gap?" *The Astrophysical Journal* 757: 36. 10.1088/0004-637X/757/1/36.

Lattimer, James M. 2026. "Neutron Star Masses (online compilation)." https://stellarcollapse.org/nsmasses. Accessed 2026-02-18.

Lattimer, James M. and F. Douglas Swesty. 1991. "A Generalized Equation of State for Hot, Dense Matter." *Nuclear Physics A* 535: 331–376. 10.1016/0375-9474(91)90452-C.

Manchester, R. N., G. B. Hobbs, A. Teoh, and M. Hobbs. 2005. "The Australia Telescope National Facility

Pulsar Catalogue." *The Astronomical Journal* 129: 1993–2006. 10.1086/428488.

Neustadt, Jack M. M. and C. S. Kochanek. 2021. "The search for failed supernovae with the Large Binocular Telescope: a new candidate and the failed SN fraction with 11 yr of data." *Monthly Notices of the Royal Astronomical Society* 508: 516–528. 10.1093/mnras/stab2605.

O'Connor, Evan and Christian D. Ott. 2010. "A new open-source code for spherically symmetric stellar collapse to neutron stars and black holes." *Classical and Quantum Gravity* 27: 114103. 10.1088/0264-9381/27/11/114103.

Oppenheimer, J. R. and G. M. Volkoff. 1939. "On Massive Neutron Cores." *Physical Review* 55: 374–381. 10.1103/PhysRev.55.374.

Özel, Feryal, Dimitrios Psaltis, Ramesh Narayan, and Jeffrey E. McClintock. 2010. "The Black Hole Mass Distribution in the Galaxy." *The Astrophysical Journal* 725: 1918–1927. 10.1088/0004-637X/725/2/1918.

Sautron, Mattéo, Jérôme Pétri, Dipanjan Mitra, and Ludmilla Dirson. 2024. "The Galactic population of canonical pulsars. II. Taking into account several evolutionary paths: Interstellar medium interaction, Galactic potential, and a death valley." *Astronomy & Astrophysics* 691: A349. 10.1051/0004-6361/202451097.

Shen, H., H. Toki, K. Oyamatsu, and K. Sumiyoshi. 1998. "Relativistic equation of state of nuclear matter for supernova and neutron star." *Nuclear Physics A* 637: 435–450. 10.1016/S0375-9474(98)00236-X.

Smartt, Stephen J. 2015. "Observational constraints on the progenitors of core-collapse supernovae: the case for missing high-mass stars." *Publications of the Astronomical Society of Australia* 32: e016. 10.1017/pasa.2015.17.

Smartt, Stephen J., John J. Eldridge, R. Mark Crockett, and Justyn R. Maund. 2009. "The death of massive stars – I. Observational constraints on the progenitors of Type II-P supernovae." *Monthly Notices of the Royal Astronomical Society* 395: 1409–1437. 10.1111/j.1365-2966.2009.14506.x.

Steiner, Andrew W., Tobias Fischer, and Matthias Hempel. 2013. "Core-collapse supernova equations of state based on neutron star observations." *The Astrophysical Journal* 774: 17. 10.1088/0004-637X/774/1/17.

Sukhbold, Tuguldur, Thomas Ertl, S. E. Woosley, Justin M. Brown, and H.-Thomas Janka. 2016. "Core-Collapse Supernovae from 9 to 120 Solar Masses Based on Neutrino-powered Explosions." *The Astrophysical Journal* 821: 38. 10.3847/0004-637X/821/1/38.

The LIGO Scientific Collaboration, The Virgo Collaboration, and The KAGRA Collaboration. 2023. "GWTC-3: Compact Binary Coalescences Observed by LIGO and Virgo During the Second Part of the Third Observing Run." *Physical Review X* 13: 041039. 10.1103/PhysRevX.13.041039.

Tolman, Richard C. 1939. "Static Solutions of Einstein's Field Equations for Spheres of Fluid." *Physical Review* 55: 364–373. 10.1103/PhysRev.55.364.

Typel, Stefan, Gerd Röpke, Thomas Klähn, David Blaschke, and Hermann H. Wolter. 2010. "Composition and thermodynamics of nuclear matter with light clusters." *Physical Review C* 81: 015803. 10.1103/PhysRevC.81.015803.

Woosley, S. E., A. Heger, and T. A. Weaver. 2002. "The evolution and explosion of massive stars." *Reviews of Modern Physics* 74: 1015–1071. 10.1103/RevModPhys.74.1015.

Zevin, Michael, Mario Spera, Christopher P. L. Berry, and Vicky Kalogera. 2020. "Exploring the Lower Mass Gap and Unequal Mass Regime in Compact Binary Evolution." *The Astrophysical Journal Letters* 899: L1. 10.3847/2041-8213/aba74e.